Monovalent Cation Permeation through the Connexin40 Gap Junction Channel

Cs, Rb, K, Na, Li, TEA, TMA, TBA, and Effects of Anions Br, Cl, F, Acetate, Aspartate, Glutamate, and NO_3

Dolores A. Beblo and Richard D. Veenstra

From the Department of Pharmacology, SUNY Health Science Center at Syracuse, Syracuse, New York 13210

ABSTRACT The unitary conductances and permeability sequences of the rat connexin40 (rCx40) gap junction channels to seven monovalent cations and anions were studied in rCx40-transfected neuroblastoma 2A (N2A) cell pairs using the dual whole cell recording technique. Chloride salt cation substitutions (115 mM principal salt) resulted in the following junctional maximal single channel current-voltage relationship slope conductances (γ_j in pS): CsCl (153), RbCl (148), KCl (142), NaCl (115), LiCl (86), TMACl (71), TEACl (63). Reversible block of the rCx40 channel was observed with TBA. Potassium anion salt γ_j are: Kglutamate (160), Kacetate (160), Kaspartate (158), KNO_3 (157), KF (148), KCl (142), and KBr (132). Ion selectivity was verified by measuring reversal potentials for current in rCx40 gap junction channels with asymmetric salt solutions in the two electrodes and using the Goldman-Hodgkin-Katz equation to calculate relative permeabilities. The permeabilities relative to Li^+ are: Cs^+ (1.38), Rb^+ (1.32), K^+ (1.31), Na^+ (1.16), TMA^+ (0.53), TEA^+ (0.45), TBA^+ (0.03), Cl^- (0.19), glutamate$^-$ (0.04), and NO_3- (0.14), assuming that the monovalent anions permeate the channel by forming ion pairs with permeant monovalent cations within the pore thereby causing proportionate decreases in the channel conductance. This hypothesis can account for why the predicted increasing conductances with increasing ion mobilities in an essentially aqueous channel were not observed for anions in the rCx40 channel. The rCx40 effective channel radius is estimated to be 6.6 Å from a theoretical fit of the relationship of relative permeability and cation radius.

KEY WORDS: gap junctions • conductance • selectivity • permeability

INTRODUCTION

Gap junction channels are formed by twelve connexin protein subunits, six in each cell membrane (Peracchia, 1973; Caspar et al., 1977; Makowski et al., 1977), which allow the cell-to-cell passage of ions and small molecules (Bennett and Spray, 1965; Loewenstein, 1981; Hertzberg and Johnson, 1988; Beyer, 1993). Connexins contain highly conserved transmembrane and extracellular domains, but unique cytoplasmic regions (Beyer and Veenstra, 1994). To date at least 16 different connexin channels have been identified which are classified according to their molecular mass. What little is known about their functional differences is limited primarily to a comparison of their unitary conductances, voltage-dependent gating properties, or regulation by intracellular kinases, protons, and calcium. These unique physiological properties are attributed to the connexin-specific differences in primary amino acid sequences (Spray and Burt, 1990). In this study, the conductance and selectivity sequences of rat connexin40 (rCx40, molecular mass ≈40 kD)[1] gap junction channels are investigated. Cx40 was chosen because it is highly expressed in Purkinje fibers, atrial myocardium, sinoatrial node, and cardiac atrioventricular conduction system in relative abundance while connexin43 (Cx43), another cardiovascular connexin, is highly expressed in ventricular myocardium and coexpressed with Cx40 in Purkinje fibers, atrial myocardium, and vascular endothelium and smooth muscle (Gourdie et al., 1993; Davis et al., 1994). These expression patterns are of particular physiological relevance since the conduction properties of these tissues vary, and it is known that Cx40 and Cx43 are not capable of forming heteromeric or heterologous gap junction channels (Bruzzone et al., 1993; Davis et al., 1994). What role the distinct channel properties of Cx40 and Cx43 play in the conduction properties of the respective tissues is not understood since relatively little is known about the dis-

Address correspondence to Dr. Dolores A. Beblo, Department of Pharmacology, SUNY Health Science Center at Syracuse, 750 East Adams Street, Syracuse, NY 13210. Fax: 315-464-8014.

[1] *Abbreviations used in this paper:* N2A, neuroblastoma 2A; rCx40, rat connexin40.

tinct permeability properties of these two major cardiovascular connexins.

While ion selectivity and permeation have been studied extensively in a variety of membrane channels (Myers and Haydon, 1972; Hille, 1975; Eisenman et al., 1978; Adams et al., 1980; Dwyer et al., 1980; Blatz et al., 1984; Hess et al., 1986; Bormann et al., 1987; Franciolini and Nonner, 1987, 1994), the ionic permeabilities of connexin channels remain relatively unknown. Typically, much less is known about ion transfer in channels permeable to both cations and anions relative to cation-selective or anion-selective channels. The anion-to-cation selectivity of these channels as determined by asymmetric salt reversal potential measurements is usually not high, which may lead to the conclusion that the ability of these channels to transport ions of any valence is due to the relatively large diameter of the pores, although accounts of more complex ion–ion and ion–site interactions do exist (Franciolini and Nonner, 1994; Borisova et al., 1986). Gap junction channels with estimated pore radii ≥5 Å fall into this class. Experimental measurements of the relative ionic permeabilities from reversal potential measurements provide a theoretical method for determining the mechanism of selectivity or lack thereof. These measurements provide functional information necessary for structure-function analysis of the channel and the mechanisms that account for its selective permeability.

In this study, as in the preceding manuscript on the rat Cx43 channel (Wang and Veenstra, 1997, appearing in this issue), we used the dual whole cell recording technique to obtain single rCx40 gap junction channel currents. Using asymmetric ionic electrode solutions in each cell of an attached pair, we determined the relative permeability from the change in reversal potential measured with LiCl as the major salt in one electrode and with each of the seven cations, Cs^+, Rb^+, K^+, Na^+, TMA^+, TEA^+, and TBA^+ as the test cation (as the Cl^- salt) in the second electrode. The ionic permeabilities were compared to the conductance ratios measured with symmetric solutions. We estimated the limiting pore radius of the rCx40 channels from the relationship between the relative ionic permeabilities and the effective ionic radii for the monovalent alkali cations and the organic alkylammonium ions TMA^+, TEA^+, and TBA^+. Only minor differences were noted in the cation conductance and permeability ratios of the rCx40 channel relative to the rCx43 channel, however, the estimates of pore radii and anionic permeability sequences suggest different mechanisms of counterion transport could be involved for these two connexin channels. These data indicate that the molecular composition and macromolecular permeability of the connexin pores could be more variable than previously thought.

METHODS

Cell Culture and Transfection

Genomic DNA containing the coding sequence of rat Cx40 was cloned into the EcoRI site of the eukaryotic expression vector pSFFV-neo and transfected into mouse Neuro2A (N2A) neuroblastoma cells as described previously (Beblo et al., 1995). N2A cell cultures were maintained as in the preceding manuscript (Wang and Veenstra, 1997).

Electrophysiological Recordings and Solutions

rCx40 connexin-transfected N2A cell cultures were plated at low density (2×10^5 cells/35 mm dish) for 24 h, washed with HEPES-buffered saline (in mM: 142 NaCl, 1.3 KCl, 0.8 $MgSO_4$, 0.9 NaH_2PO_4, 1.8 $CaCl_2$, 5 CsCl, 2 TEACl, 5.5 dextrose, and 10 HEPES, pH 7.4) and examined electrophysiologically on the stage of an inverted phase-contrast light microscope (IMT-2; Olympus Corp., Lake Success, NY). The compositions of the IPSs and bath solution are listed in Table I. The osmolarity of all IPS and bath solutions (310 ± 5 mosm) were measured before each experiment (Model 3W2 osmometer; Advanced Instruments Inc., Needham Heights, MA), and all experiments were performed at room temperature (20–22°C). The manufacture of the patch electrodes and analysis of junctional currents were performed following the same procedures described in the preceding manuscript (Wang and Veenstra, 1997). Double whole cell patch clamp recordings were obtained using two Axopatch-1D amplifiers (Axon Instruments, Inc., Foster City, CA). All current and voltage records were stored on VCR tape using a 4-channel digitizing unit (DR-484 Neuro-corder; Neuro Data Instruments Corp., NY) and VCR tape recorder (JVC HR-D600U) for off-line analysis.

Channel Current Analysis

Junctional channel currents were displayed as paired whole cell currents or as individual ΔI_2 traces. All points current amplitude histograms were compiled from the $-\Delta I_2$ ($\approx I_j$) trace for each experiment (Veenstra and Brink, 1992). Off-line analysis was completed following the same procedures described in the preceding manuscript (Wang and Veenstra, 1997) using the DOSTAT analysis software (Brink and Fan, 1989; Manivannan et al., 1992; Ramanan and Brink, 1993).

Cation and Anion Selective Permeability Calculations

To measure ionic selectivity reversal potentials for junctional currents in rCx40 gap junction channels were determined with 10 different asymmetric salt solution sets. Since each solution contained several ions (Table I), E_{rev} is a function of all ion permeabilities according to the Goldman-Hodgkin-Katz voltage equation (see Wang and Veenstra, 1997). The ionic permeability ratios (P_{ion}/P_{Li}, see Table V) were calculated simultaneously using a matrix which contained the concentrations and ionic reversal potentials for all asymmetric solutions. The set of permeability ratios satisfied all of the E_{rev} data listed in Table IV. Divalent cations, Mg^{2+} and Ca^{2+}, which constituted <3% of the IPS ionic concentration (Table I), were constant in all IPSs with the exception of IPS KF due to precipitation and were neglected in all calculations.

TABLE I

Ionic Composition of Bath and Internal Pipette Solutions (IPS, mM)

Component (mM)	Cation chloride salt IPSs								Potassium anion salt IPSs						
	CsCl	RbCl	KCl	NaCl	LiCl	TMACl	TEACl	TBACl	KF	KBr	KNO_3	Kacetate	Kaspartate	Kglutamate	Bath
CsCl	120	5	5	5	5	5	5	5	5	5	5	5	5	5	5
RbCl	—	115	—	—	—	—	—	—	—	—	—	—	—	—	—
KCl	—	—	115	—	—	—	—	—	—	—	—	—	—	—	1.3
NaCl	—	—	—	115	—	—	—	—	—	—	—	—	—	—	142
LiCl	—	—	—	—	115	—	—	—	—	—	—	—	—	—	—
TMACl	—	—	—	—	—	115	—	—	—	—	—	—	—	—	—
TEACl	2	2	2	2	2	2	117	2	2	2	2	2	2	2	2
TBACl	—	—	—	—	—	—	—	115	—	—	—	—	—	—	—
KF	—	—	—	—	—	—	—	—	115	—	—	—	—	—	—
KBr	—	—	—	—	—	—	—	—	—	115	—	—	—	—	—
KNO_3	—	—	—	—	—	—	—	—	—	—	115	—	—	—	—
Kacetate	—	—	—	—	—	—	—	—	—	—	—	115	—	—	—
Kaspartate	—	—	—	—	—	—	—	—	—	—	—	—	115	—	—
Kglutamate	—	—	—	—	—	—	—	—	—	—	—	—	—	115	—
BAPTA	5	5	5	5	5	5	5	5	5	5	5	5	5	5	—
$MgCl_2 \cdot 6H_2O$	4	4	4	4	4	4	4	4	—	4	4	4	4	4	—
$CaCl_2 \cdot 2H_2O$	3	3	3	3	3	3	3	3	—	3	3	3	3	3	—
KH_2OPO_4	—	1	1	1	1	1	1	1	—	1	1	1	1	1	—
$MgSO_4 \cdot 7H_2O$	—	—	—	—	—	—	—	—	—	—	—	—	—	—	0.811
$NaH_2PO_4 \cdot H_2O$	—	—	—	—	—	—	—	—	—	—	—	—	—	—	0.942
Dextrose	—	—	—	—	—	—	—	—	—	—	—	—	—	—	5.55
$CaCl_2$	—	—	—	—	—	—	—	—	—	—	—	—	—	—	1.8
Hepes	25	25	25	25	25	25	25	25	25	25	25	25	25	25	9.99
Na_2ATP	3	3	3	3	3	3	3	3	3	3	3	3	3	3	—
Na_2CP	3	3	3	3	3	3	3	3	3	3	3	3	3	3	—
Osmolarity (mosm)	310	310	310	310	310	310	310	310	295	310	310	310	310	310	310
pH	7.0	7.0	7.0	7.0	7.0	7.0	7.0	7.0	7.0	7.0	7.0	7.0	7.0	7.0	7.0

RESULTS

Single Channel Cation Chloride Salt Conductances

The single channel current amplitudes of the rCx40 channel were measured under symmetric salt conditions for all test monovalent cations. Fig. 1 *A* shows a segment of a double whole cell recording of a rCx40 channel in IPS KCl during a 2-min, −40-mV transjunctional voltage (V_j) pulse. The current amplitude of each channel recording is obtained by fitting the all points (real time) histogram of the $-\Delta I_2$ trace with a probability density function (pdf) as illustrated in Fig. 1 *B*. To illustrate the symmetry of the rCx40 channel current amplitude with respect to V_j, the current recording and histogram of the same rCx40 channel obtained at +40 mV are also illustrated in Fig. 1, *C* and *D*. Junctional channel current amplitudes (i_j) for each V_j are plotted in Fig. 1 *E*, and the linear regression fit of the single rCx40 channel current-voltage relationship yielded a single channel slope conductance (γ_j) for this cell pair of 139 pS ($r = 0.99$).

The IPS KCl single channel current-voltage relationships from six different cell pairs were pooled together and a linear regression analysis of the composite i_j-V_j relation produced a slope conductance of 141.5 pS (Fig. 2 *C*). This is comparable to the mean value γ_j of 141.2 ± 4.4 pS calculated from the independent slope conductances of the six IPS KCl rCx40 cell pairs (137.8, 137.5, 147.4, 146.2, 138.7, 139.3). These procedures were repeated for the other test cations and the i_j-V_j relationships for each test solution are illustrated in Fig. 2. The number of cell pairs, slope conductance of the composite i_j-V_j relations, and the mean conductance obtained from the linear slopes of the individual i_j-V_j relations are summarized in Table II.

TBA rCx40 Channel Block

In six cell pairs during more than 44 min of recording currents at various transjunctional voltages with 115 mM TBACl in both cell pipettes, junctional coupling was absent with the exception of two short duration (<50 ms) channel openings in one cell pair. To verify

that TBA was blocking the rCx40 channel rather than affecting the recordings through nonspecific junctional or nonjunctional effects (i.e., seal breakdown), TBACl was added to only one pipette in decreasing concentrations until the presence or absence of junctional current activity could be verified using IPS KCl. With 115 mM TBA in one pipette and 115 mM KCl in the other, nonjunctional currents (as indicated by the lack of equal and opposite polarity currents in both cells) were observed in the TBACl cell when a V_j was applied such that TBA was driven into the channel. This occurred in conjunction with TBA cell swelling and KCl cell shrinkage.

In the presence of 5 mM TBACl, V_j polarity was varied in a stepwise manner, and the resultant junctional current activity was recorded. Fig. 3 *A* demonstrates the presence of junctional current activity during $+V_j$ pulses and disappearance of the same channel activity during $-V_j$ pulses. The V_j transitions from +35 to −40 mV and from −40 to +25 mV are illustrated at higher time resolution in Fig. 3, *B* and *C*, which indicates the disappearance of and recovery of discrete channel openings. The i_j-V_j relationship for this experiment is shown in Fig. 3 *D*. The γ_j of 141 pS is equal to the mean conductance obtained with symmetric IPS KCl which is consistent with an insignificant TBA current. The V_j-dependent kinetics of the onset and removal of apparent TBA block were not examined in this investigation.

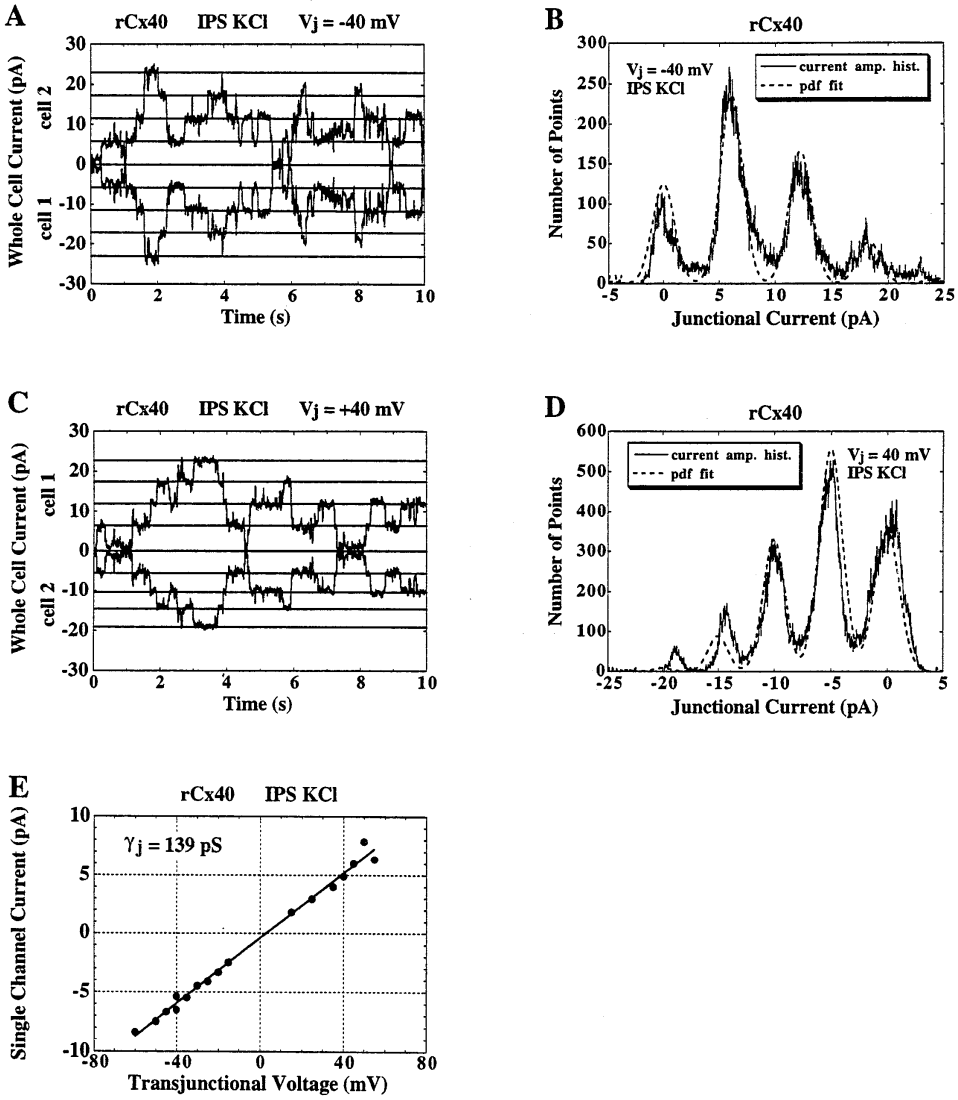

FIGURE 1. Rat connexin40 single channel activity with IPS KCl (Table I). (*A*) Whole cell currents from a rat Cx40 transfected N2A cell pair during a −40-mV step applied to cell 1 from a common holding potential of 0 mV, resulting in a transjunctional voltage (V_j) of −40 mV. Junctional currents appear as opposite polarity signals. A 10-s interval of a 120-s recording is shown to illustrate the closed (ground, $I_j = 0$) state and open states of the four channels observed during the pulse. Both current traces were low pass filtered at 40 Hz and digitized for illustration at 1 kHz. (*B*) All points histogram (*solid line*) compiled from the cell 2 current trace. The first 10 s of the recording were omitted due to nonstationary channel activity. The parameters for the probability density function (pdf, *dashed line*) include four channels each with a single channel current of 6.1 pA (152.5 pS), 0.32 open probability, and closed and open state current variances of 0.5 pA. (*C*) Whole cell currents from the same cell pair as *A* during a +40-mV step applied to cell 1. This current trace also shows four open channels, each with a single channel current of 5 pA (125 pS). (*D*) All points histogram of the cell 2 current trace shown in *C*. Each channel had an open probability of 0.27 and current variance of 0.4 pA. The closed state current variance was 0.55 pA. (*E*) Single channel current-voltage relationship for the same cell pair illustrated in *A* and *C*. Each dot represents the junctional current amplitude of an observed channel for an applied V_j pulse. The single channel slope conductance (γ_j) of 139 pS was determined from the linear regression fit (*solid line*) of the data ($r > 0.99$).

Single Channel Potassium Anion Salt Conductances

Equimolar ion substitution of seven different anions (Cl^-, Br^-, glutamate$^-$ plus F^-, NO_3^-, acetate$^-$, and aspartate$^-$, all 115 mM K^+ salts) were also performed using identical procedures to those described above for cations. The single channel currents were analyzed as presented above, and the i_j-V_j relationships for each test solution are illustrated in Fig. 4. The number of cell pairs, slope conductance of the composite i_j-V_j relations, and mean slope conductance of the individual linear i_j-V_j relations are summarized in Table III. The divalent cations Mg^{2+} and Ca^{2+} and phosphate anion

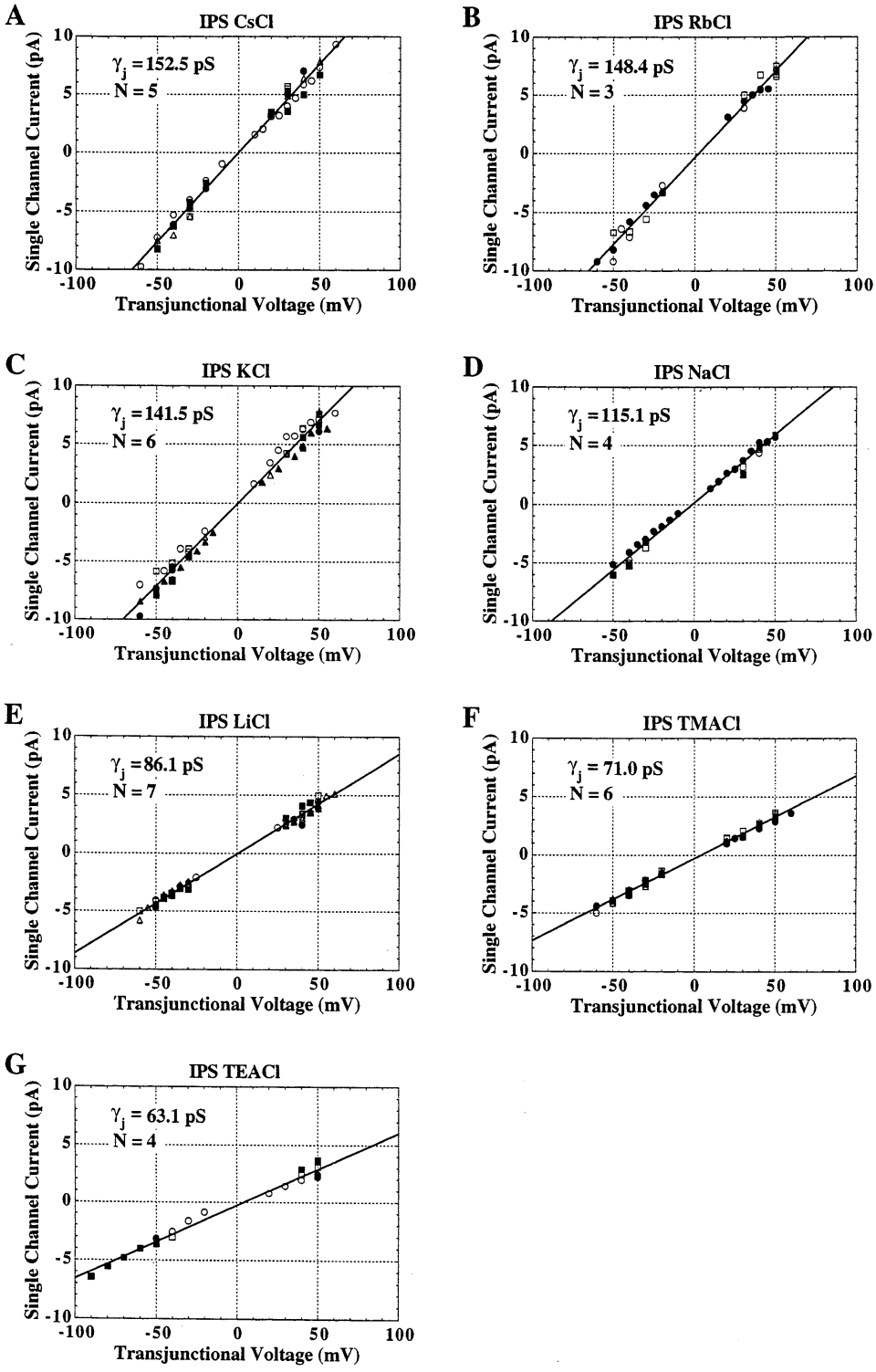

FIGURE 2. Single channel junctional current-voltage relationships using substituted cation chloride salt IPSs (Table I). Each symbol refers to a different cell pair. The composite slope conductance (γ_j) obtained by linear regression fit (*solid line*) of the single channel current amplitudes from all of the cell pairs (*N*) indicated. (*A*) IPS CsCl, γ_j = 152.5 pS, 5 cell pairs. (*B*) IPS RbCl, γ_j = 148.4 pS, 3 cell pairs. (*C*) IPS KCl, γ_j = 141.5 pS, 6 cell pairs. (*D*) IPS NaCl, γ_j = 115.1 pS, 4 cell pairs. (*E*) IPS LiCl, γ_j = 86.1 pS, 7 cell pairs. (*F*) IPS TMACl, γ_j = 71.0 pS, 6 cell pairs. (*G*) IPS TEACl, γ_j = 63.1 pS, 4 cell pairs. The slope conductances listed here are not statistically different from the mean calculated from the individual single channel junctional current-voltage relationships for each cell pair (see RESULTS). Correlation coefficients were >0.99 for all graphs.

TABLE II

Slope Conductances for Monovalent Cation Solutions

IPS	Composite γ_j (pS)	Mean $\gamma_j \pm$ SE (pS)	*n* cell pairs
CsCl	152.5	158.7 ± 6.3	5
RbCl	148.4	147.9 ± 1.0	3
KCl	141.5	141.2 ± 1.8	6
NaCl	115.1	115.8 ± 1.8	4
LiCl	86.1	86.5 ± 1.5	7
TMACl	71.0	70.6 ± 0.9	6
TEACl	63.1	61.4 ± 4.5	4

(monobasic Kphosphate) were omitted from the potassium fluoride IPS (Table I) due to problems with coprecipitation. A 6.5% reduction in total conductance was expected by these alterations. A composite slope of 148.0 pS was obtained with IPS KF. However, accounting for the reduction in osmolarity, a slope conductance of 158.3 pS was used for comparison with other test anion IPS. Phosphate also caused Cs^+ to precipitate and was omitted from IPS CsCl (Table I). This was estimated to reduce the IPS CsCl total conductance by <0.4% and was therefore neglected.

Relationship between Channel Conductance and Aqueous Mobility

The monovalent cation and anion channel conductances were plotted as a function of their aqueous mobilities in Fig. 5, *A* and *B*, respectively. For the test cations, the channel conductance-mobility plot (Fig. 5 *A*, *solid line* and *open circles*) approximates a straight line with a slope of 18.1 pS and y-intercept of 5.0 pS (r = 0.96). The y-intercept predicts the conductance of the rCx40 channel in the presence of an impermeable (inert) cation and 136 mM Cl^-, although it should be noted that 12 mM Na^+, 5 mM Cs^+, and 2 mM TEA^+ are always present in each IPS. Hence, a surprisingly low Cl^- conductance is estimated from this approach. Based on the aqueous diffusion coefficients for the test cations and Cl^- alone (i.e., no channel ionic selectivity) a line with a slope of 7.9 pS and y-intercept of 81.8 pS is predicted (*dashed lines* and *filled circles*). Clearly the difference in the two lines suggests that ions are not diffusing through the pore with the same mobility they possess in bulk solution. Even though the rCx40 channel cation conductance sequence (Table II) qualitatively matches the aqueous mobility sequence, the differences in the ionic conductance-mobility plots are indicative of a reduction of mobility created either by solvent drag within a restricted space or weak electrostatic interactions which alter the aqueous state of the ion in the pore (e.g., partial dehydration by another ion or site within the pore).

An entirely different result was obtained when the test anion channel conductances (Table III) were plotted as a function of their aqueous mobilities (Fig. 5 *B*).

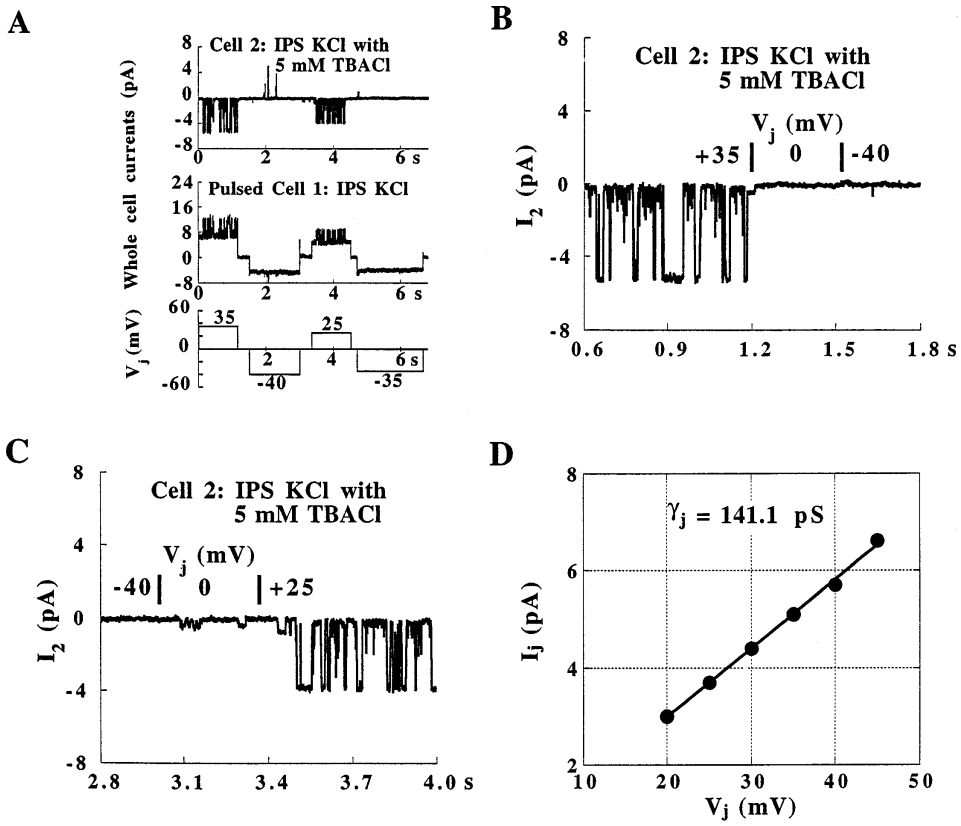

FIGURE 3. Experiments with IPS TBACl. (*A*) Whole cell currents during an experiment in which one electrode (cell 1) was filled with IPS KCl and the other (cell 2) was filled with IPS KCl in which TBACl was dissolved to yield a final concentration of 5 mM TBACl. A significantly greater number of open channel current transitions is shown during positive relative to negative polarity V_j pulses applied to cell 1. (*B*) Expanded view of *A* illustrating the disappearance of discrete channel opening from +35 to −40 mV. (*C*) Expanded view of *A* showing the recovery of discrete channel opening from −40 to +25 mV. (*D*) The i_j-V_j relationship for this experiment. The γ_j of 141 pS is equal to the mean conductance obtained with symmetric IPS KCl which is consistent with an insignificant TBA current.

Again, the predicted anion conductance-mobility plot for the test anions, based on their respective aqueous diffusion coefficients (and no channel ionic selectivity, *dashed line* and *filled circles*), is shown for comparison to the experimental results (*open circles*). The experimental data do not approximate a straight line with a positive slope as predicted by independent electrodiffusion theory. In fact, channel conductance remains essentially constant over a wide range of anionic aqueous mobilities with the exception of Cl^- and Br^-, where the conductance unexpectedly decreases. In a relatively nonselective pore with weak cation–anion and ion–site

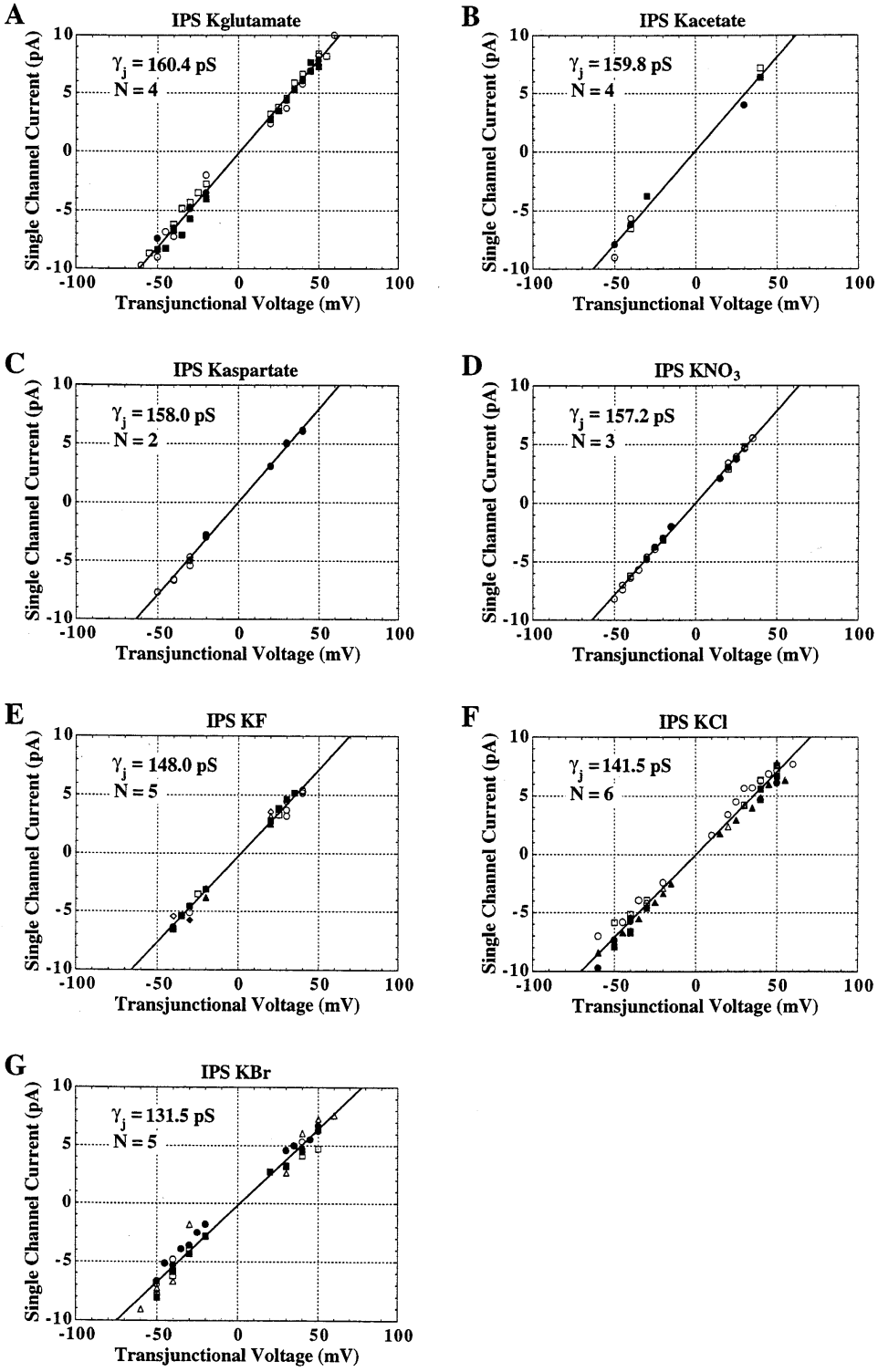

FIGURE 4. Single channel junctional current-voltage relationships using substituted anion potassium salt IPSs (Table I). Each symbol refers to a different cell pair. The composite slope conductance (γ_j) obtained by linear regression fit (*solid line*) of the single channel current amplitudes from all of the cell pairs (*N*) indicated. (*A*) IPS Kglutamate, γ_j = 160.4 pS, 4 cell pairs. (*B*) IPS Kacetate, γ_j = 159.8 pS, 4 cell pairs. (*C*) IPS Kaspartate, γ_j = 158.0 pS, 2 cell pairs. (*D*) IPS KNO_3, γ_j = 157.2 pS, 3 cell pairs. (*E*) IPS KF, γ_j = 148.0 pS, 5 cell pairs. (*F*) IPS KCl, γ_j = 141.5 pS, 6 cell pairs. (*G*) IPS KBr, γ_j = 131.5 pS, 5 cell pairs. The slope conductances listed here are not statistically different from the mean calculated from the individual single channel junctional current-voltage relationships for each cell pair (see RESULTS). Correlation coefficients were >0.99 for all graphs.

interactions as expected from the cation conductance sequence, Cl^- and Br^- should be more permeable than the other anions and, thus, produce a larger unitary current and channel conductance. Because of these initial rCx40 channel conductance measurements with Br^-, Cl^-, acetate$^-$, and glutamate$^-$, we also tested F^-, nitrate$^-$, and aspartate$^-$ which yielded identical results. Since the anion conductance mobility plot produced an inverse relation to the aqueous mobility sequence, the Levitt approximation for estimating the reduction in ionic mobilities within the pore relative to bulk solution, as applied to the rCx43 channel (Wang and Veenstra, 1997), was not attempted for the rCx40 channel.

Relative Ion Permeability Ratios and Estimation of Pore Size

The monovalent cation and anion conductance ratios suggest that there are weak cation interactions within the rCx40 pore. Yet some highly selective mechanism which paradoxically reduces channel conductance for Cl^- and Br^- and permits an essentially constant (and higher) conductance in the presence of larger organic anions or F^- (a more hydrated anion) also exists. To determine whether the rCx40 channel's relative ionic permeabilities actually correlate with the relative channel conductance measurements, reversal potentials were measured from i_j-V_j relationships in cell pairs that were dialyzed with different IPSs on each side of the junction. In a series of experiments, the asymmetric salt reversal potentials were obtained for all of the test cation-Cl salt solutions relative to 115 mM LiCl (IPS LiCl, Table I). Fig. 6 *A* illustrates the i_j-V_j relationship obtained from four cell pairs using asymmetric IPS KCl/LiCl salt gradients. V_j was defined as the voltage of the IPS KCl cell relative to the LiCl cell ($V_j = V_{KCl} - V_{LiCl}$) even though both cells were pulsed at different times during the course of each experiment. This convention is necessary to avoid transposing the measured channel current amplitudes on the voltage axis when using asymmetric salt solutions (see Wang and Veenstra, 1997). The zero current intercept of the composite linear i_j-V_j relationship equals the reversal potential (E_{rev}) for the cell pairs with opposing K^+ and Li^+ concentration gradients and is in close agreement with the mean E_{rev} of $+5.0 \pm 0.9$ mV (mean ± SE) determined from the E_{rev} of each of the four experiments. E_{rev} was determined with each asymmetric solution set using the identical protocol illustrated in Fig. 6 *A*; the results are summarized in Table IV.

To determine the permeability ratio P_{Cl}/P_{Li}, E_{rev} was also obtained with different concentrations of LiCl on each side of the junction. One pipette contained 115 mM LiCl (IPS LiCl) and the other pipette a solution with

TABLE III

Slope Conductances for Monovalent Anion Solutions

IPS	Composite γ_j (pS)	Mean $\gamma_j \pm$ SE (pS)	*n* cell pairs
Kglutamate	160.4	160.4 ± 2.4	4
Kacetate	159.8	159.8 ± 6.2	4
Kaspartate	158.0	158.0 ± 0.0	2
KNO_3	157.2	155.1 ± 2.3	3
KF	148.0	149.5 ± 3.7	5
KCl	141.5	141.2 ± 1.8	6
KBr	131.5	131.2 ± 2.5	5

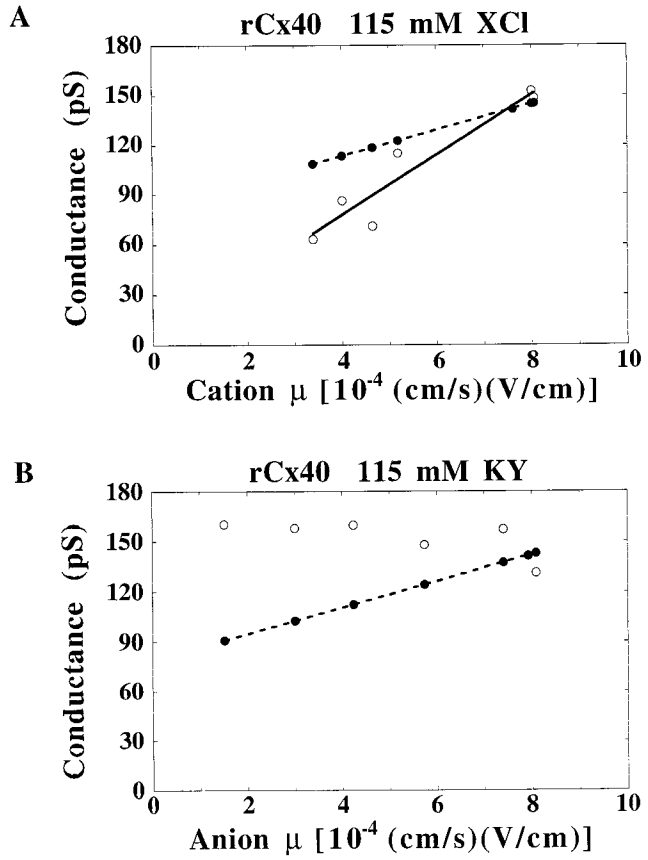

FIGURE 5. Comparison of theoretical aqueous and junctional rCx40 single channel conductances. The theoretical linear relationships (*dashed lines*) of the conductance with mobility were calculated from the Goldman-Hodgkin-Katz current equation assuming ion permeabilities directly proportional to their diffusion coefficients. (*A*) Junctional (*open circles*) and theoretical (*filled circles*) aqueous relative single channel conductance are plotted versus cation mobility. The relationship of junctional conductance with cation mobility was fit by linear regression (*solid line*, $r = 0.96$). The conductance sequence $Cs^+ > Rb^+ > K^+ > Na^+ > Li^+ > TMA^+ > TEA^+$ resulted from the cation-Cl substitutions. (*B*) Junctional (*open circles*) and theoretical (*filled circles*) aqueous relative single channel conductance are plotted versus anion mobility. The relationship of junctional conductance ratios with anion mobility decreased only slightly up to a mobility of 7.4×10^{-4} cm^2/V·s but declined sharply for greater mobilities. This was in marked contrast to the linearly increasing conductance ratios predicted for an aqueous channel (*dashed line*).

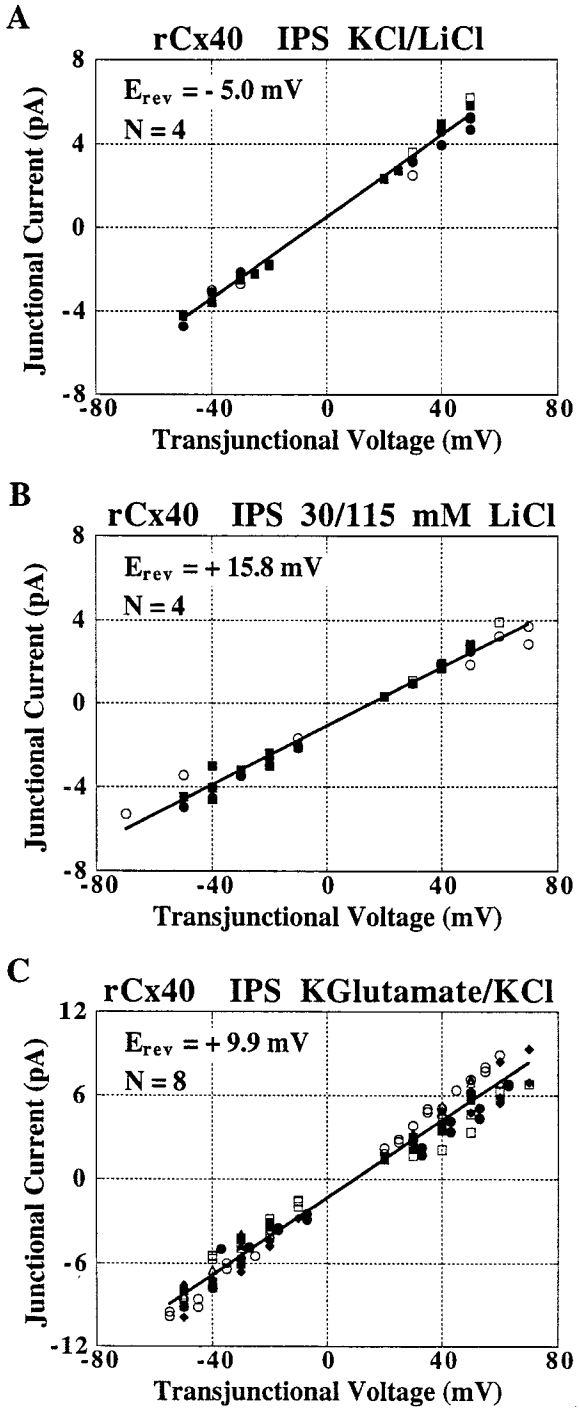

FIGURE 6. (*A*) Single channel current-voltage relationships obtained for the purpose of determining reversal potentials to confirm the relative conductances measured with the symmetric salt solutions. I_j-V_j relationships from four cell pairs using asymmetrical 115 mM KCl/LiCl IPSs. The linear regression fit (*solid line*, r = 0.99) of all channel current amplitudes indicates a reversal potential (I_j = 0) of 9.9 mV. (*B*) Single channel junctional current-voltage relationships obtained for the purpose of determining the rCx40 relative permeabilities of Li^+ and Cl^-. The i_j-V_j relationships (n = 4) were determined when one cell of a rCx40 transfected N2A cell pair was dialyzed with IPS LiCl (115 mM LiCl) and the other cell of the pair with a lower LiCl concentration (30 mM) and mannitol (145 mM) for osmotic balancing. The linear regression fit (*solid line*, r = 0.99) of all channel current amplitudes indicates a reversal potential (I_j = 0) of 15.8 mV. (*C*) I_j-V_j relationships from four cell pairs using asymmetrical 115 mM Kglutamate/KCl IPSs. The linear regression fit (*solid line*, r = 0.99) of all channel current amplitudes indicates a reversal potential (I_j = 0) of 9.9 mV.

TABLE IV

Reversal Potentials

IPS sets	n	E_{rev} ± SE (mV)	Composite E_{rev}
IPS CsCl/LiCl	3	−6.1 ± 1.3	−5.9
IPS RbCl/LiCl	3	−5.1 ± 2.3	−5.1
IPS KCl/LiCl	4	−5.0 ± 0.9	−5.0
IPS NaCl/LiCl	3	−2.2 ± 0.9	−2.8
IPS TMACl/LiCl	3	10.6 ± 0.7	10.2
IPS TEACl/LiCl	2	12.8 ± 0.9	12.5
IPS KCl/KCl with 5 mM TBACl	2	3.1 ± 0.1	2.9
IPS LiCl/30 mM LiCl and mannitol	4	16.1 ± 0.2	15.8
IPS KG/KCl	8	10.3 ± 1.0	9.9
IPS KNO_3/KCl	2	1.1 ± 0.2	0.9

the LiCl reduced to 30 mM and mannitol (145 mM) added to maintain osmotic balance with IPS LiCl. All other ionic components of the IPS remained unaltered.

Fig. 6 *B* illustrates the composite i_j-V_j relationship obtained from six cell pairs with asymmetric LiCl solutions. The E_{rev}s for each set of asymmetric solution experiments are listed in Table IV. To test whether mannitol permeates the rCx40 channel, one additional experiment was performed in which stachyose, a tetrasaccharide, replaced mannitol as the IPS osmotic balancing agent. The reversal potential of 16.3 mV with stachyose compared well with the average reversal potential measured with mannitol of 16.1 mV as listed in Table IV.

Asymmetric salt reversal potential experiments were also performed on two of the organic anions with the highest and lowest aqueous diffusion coefficients (∝ aqueous mobilities), nitrate$^-$ and glutamate$^-$, to determine their permeabilities relative to Cl^-. Fig. 6 *C* illustrates the composite i_j-V_j relationship obtained from five cell pairs with asymmetric IPS Kglutamate/KCl gradients across the junction.

Ionic relative permeabilities were determined using the Goldman-Hodgkin-Katz voltage equation (see Eq. 3 of Wang and Veenstra, 1997). For comparison, the junctional conductance ratios, theoretical aqueous permeabilities, and ionic permeability coefficients relative to Li^+ are all listed in Table V. The permeability and conductance ratios both agree qualitatively with the relative cation mobility sequence of $Cs^+ > Rb^+ > K^+ > Na^+ > Li^+ > TMA^+ > TEA^+$. This permeability sequence cor-

TABLE V

Comparison of rCx40 Gap Junction Relative Ion Permeability, rCx40 Conductance, and Aqueous Diffusion Coefficient Ratios

X (Y)	$P_{X\text{ or }Y}/P_{Li}$ (P_Y/P_{Cl})	$\gamma_{XCl}/\gamma_{LiCl}$ (γ_{KY}/γ_{KCl})	$D_{X\text{ or }Y}/D_{Li}$ (D_Y/D_{Cl})
Cs^+	1.38	1.77	2.00
Rb^+	1.32	1.72	2.01
K^+	1.31	1.64	1.90
Na^+	1.16	1.34	1.29
Li^+	1.00	1.00	1.00
TMA^+	0.53	0.82	1.16
TEA^+	0.45	0.73	0.84
TBA^+	0.03	—	—
(Cl^-)	0.19 (1.00)	(1.00)	1.97 (1.00)
(NO_3^-)	0.25 (1.32)	(1.11)	1.84 (0.94)
(Glutamate$^-$)	1.02 (5.28)	(1.13)	0.38 (0.19)

responds to an Eisenman I sequence. The observation that the permeability and conductance ratios calculated are significantly lower than the aqueous diffusion coefficient ratios suggests that there is some finite interaction (e.g., partial dehydration or steric hindrance) occurring between the monovalent cations and the pore of the rCx40 gap junction channel.

Channel radii have been estimated previously from permeability ratios (Renkin, 1954; Levitt, 1975, 1991; Dwyer et al., 1980) assuming a cylindrical mechanical pore model with radius *r*. The permeability ratios are described as a function of the radii ratio α, which is defined as *a*/*r*, where *a* is the ion spherical radius. Drag factors as a function of *a* or α have also been considered. We have applied the following function which is a solution to the hydrodynamic continuum equation (Dwyer et al., 1980) assuming that the ion travels along the axis in an infinite uniform cylinder:

$$P_X/P_{Li} = C(1-\alpha)^2\,[1 - 2.105\alpha + 2.0865\alpha^3 - 1.7068\alpha^5 + 0.72603\alpha^6/(1 - 0.75857\alpha^5)],$$

for a chi-squared fit of P_X/P_{Li} as shown in Fig. 7. The quantity $C(1-\alpha)^2$ represents a volume displacement term which estimates the effective target areas for ion entry into the pore relative to their respective cross-sectional areas. The best fit of the permeability data was obtained with $C = 32.6$ and an estimated pore radius of 6.6 ± 0.7 Å (mean ± standard error of pore radius determined by chi-squared fit of the data).

DISCUSSION

The purpose of this investigation was to determine the monovalent cation and anion selectivity of the rCx40 gap junction channel. In addition to electrostatic interactions at specific pore sites where the ion could be temporarily bound or be repulsed by like charges, other factors affecting ion permeability include increasing binding affinity (decreasing hydration) and pore size. Ion diffusion in a pore is classically described as being inversely related to frictional drag which depends on the ratio of the effective ion radius to the limiting pore radius (Anderson and Quinn, 1974; Levitt, 1975). If current is forced to flow by an applied voltage, electro-osmosis occurs whereby moving ions drag water molecules. Removal of water molecules from permeant ions (hydration-dehydration rates) and channel transformation (e.g., conductance state and kinetics) during ion transit may also affect permeability (Hille, 1992).

For many ion channels, ion permeation deviates from classical electrodiffusion theory due to loss of independence (ion–ion interactions) and binding or repulsion from specific sites within the pore (ion–site interactions). These interactions are enhanced by restricted space at the site of these interactions. As a consequence, the single channel conductance sequences

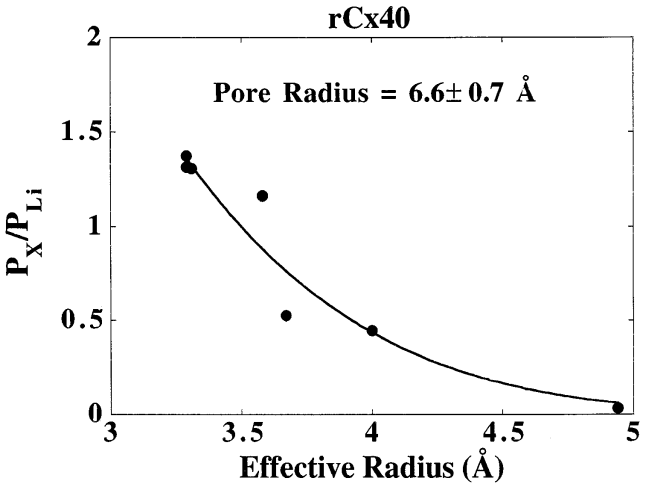

FIGURE 7. Relationship between rCx40 gap junction channel relative ion permeability (P_X/P_{Li}) as listed in Table V and hydrated radius (Nightingale, 1959) for the monovalent cations studied. The theoretical fit of the hydrodynamic equation suggests a pore radius of 6.6 ± 0.7 Å.

and permeability sequences for a series of ions are not necessarily correlated. The lack of correspondence can occur in saturating systems because two coefficients, a binding constant and a rate constant, are necessary to define conductance. In contrast, only one constant (the product of the binding constant and rate constant) is needed to define permeability (Eisenman et al., 1978). Hess et al. (1988) reported that the monovalent cation sequence from E_{rev} measurements stands in contrast to single channel conductance for Ca^{2+} channels in isolated guinea pig cardiac ventricular myocytes. Thus, it is necessary to obtain an independent measure of relative permeability, by measuring reversal potentials under asymmetric salt conditions, and/or by directly testing for independence (e.g., saturation etc.). These circumstances might be relevant to gap junctions because their limiting channel radii of ≥5 Å are presumed to accommodate both anions and cations simultaneously. Furthermore, the gap junction channel is a long pore with a length ≥150 Å. Flux coupling, a result of crowded conditions in a long, narrow pore, can reduce the effective mobility of each permeant ion, although this concept has not been generally applied to gap junctions. The permeability and conductance behavior produced by ion–ion interactions can manifest themselves as concentration-dependent permeability ratios (Sandblom et al., 1977; Eisenman et al., 1978) and "anomalous mole-fraction dependent" conductances (Andersen, 1975; Neher, 1975).

The two methods applied in this study are commonly used to determine ionic selectivity from voltage clamp measurements. The first method, comparing the conductance in a test and control solution, requires that the conductance measured with each solution corresponds to the same conductance state of each channel, and that there is no saturation or block of open channels by any ion in solution. In this investigation we used maximum single channel conductances. The second method uses the asymmetric salt reversal potential, obtained from plots of single channel peak current versus voltage, and the Goldman-Hodgkin-Katz voltage equation. Reversal potential measurements are not affected by the number of conducting channels, block, or simple saturation. Diffusion potential errors were minimized for all cation reversal potential experiments by keeping Cl^- constant (136 mM) in the Ag/AgCl half-cell reactions. Any offset potentials between the recording electrodes and ground were compensated by the junction potential potentiometer of the patch clamp amplifier before GΩ seal formation. Larger electrode offset potentials resulting from anion substitution, since Cl^- was reduced to 21 mM in these cases, were similarly compensated before GΩ seal formation and subsequent whole cell recording (see Wang and Veenstra, 1997). Hence, the asymmetric salt reversal potential of the corresponding i_j-V_j relationship reflects the differences in ionic permeabilities across the rCx40 junction.

These results demonstrate that the conductance and permeability sequences for monovalent cations and anions are identical ($Cs^+ > Rb^+ > K^+ > Na^+ > Li^+ > TMA^+ > TEA^+ > TBA^+$ and glutamate$^- \geq$ acetate$^- \geq$ aspartate$^- \geq$ nitrate$^- > F^- > Cl^- > Br^-$). The cation sequence also follows the aqueous mobility sequence for the test cations with the exception of TMA^+ being less permeable than Li^+. This is equivalent to the Eisenman I sequence and suggests only weak electrostatic interactions with other ions with charged sites within the rCx40 pore. This is in slight contrast to the Eisenman II sequence observed for the rCx43 pore (Wang and Veenstra, 1997), although neither pore possesses a pronounced affinity for the monovalent cations as evidenced by their conductance and permeability sequences. The most notable difference between the rCx40 and rCx43 channels is in the relative conductance and permeability ratios for Li^+ and Na^+. In the rCx40 channel the conductance and permeability ratios of Li^+ were less than those of Na^+, but both were approximately equal for Na^+ and Li^+ in the rCx43 channel. However, in neither case do the differences in conductance mimic the differences in the respective ionic aqueous mobilities. The cation conductance-mobility (γ_j-μ_{cation}) plots for the rCx40 channel suggests that channel conductance is predominantly dependent on cationic flux with ≤5 pS of total channel conductance being attributed to 136 mM Cl^- (Fig. 5 *A*). The slope of the rCx40 γ_j-μ_{cation} relationship (18 pS) is nearly double that of the rCx43 channel, indicative of a more cation selective channel. However, the rCx40 P_{Cl}/P_{Li} = 0.19 determined from the asymmetric 115/30 mM LiCl experiments with mannitol is nearly identical to the P_{Cl}/P_{Li} of 0.18 determined for the rCx43 channel using the same 115/30 mM LiCl gradient with raffinose. P_{Cl}/P_{Li} ratios were also determined using stachyose for both rCx40 and rCx43 channels with identical results to those mentioned above.

The anion conductance and permeability sequences for the rCx40 channel are in sharp contrast to the aqueous mobility sequence. As opposed to the Eisenman I permeability sequence observed for the rCx43 channel, the rCx40 channel conductance remains essentially constant at 158–160 pS for all of the non-atomic anions (glutamate$^-$, aspartate$^-$, acetate$^-$, and nitrate$^-$). Only the halide anions Br^-, Cl^-, and F^- exhibited lower γ_j values, and their values were also the reverse of what is expected from their aqueous mobilities. It should be noted that the IPS solution composition with potassium fluoride differed slightly compared to the other salts due to precipitation (Table I). The necessary conductance scaling for comparison with

other salt conductances may have affected the placement of fluoride in the overall monovalent anion sequence. The relative permeability of two oxy anions with the highest and lowest mobilities (nitrate$^-$ and glutamate$^-$) relative to Cl^- was determined to test this phenomenon based on the conductance ratio determinations. Again, the permeability coefficients determined from the asymmetric salt reversal potential experiments (Table V and Fig. 6 *C*) confirmed the findings of the conductance ratio experiments.

From these observations, two possible mechanisms could account for the observed effects of anion substitution upon rCx40 channel conductance. First, higher channel conductances were observed for the oxy anions (O = C-O$^-$ or O = N-O$^-$ groups) which suggests that these groups are preferentially conducted as indicated by the permeability coefficient calculations (Table V). However, this explanation also requires that any oxy anion has a similar conductance irrespective of the size of the entire molecule. This is not likely to occur in a partially hydrated pore and is more consistent with the general characteristics of a facilitated anion transport mechanism. An attempt was made to address the issue of oxy anion versus halide anion by performing conductance measurements with F^- since its aqueous mobility is between that of nitrate$^-$ and glutamate$^-$, but the results were inconclusive due to differences in the solubility of the various anions.

The second possible explanation is that the higher mobility anions actually do permeate through the pore of the rCx40 channel more readily than their lower mobility counterparts (nitrate through glutamate), but as a neutral ion pair associated with a permeant potassium ion, not as a counterion flow of opposite direction to the cation flux as is generally assumed for a nonselective aqueous pore. Hence, the more permeant anion reduces the total current rather than contributing to it as in the rCx43 channel. As we have proposed in the companion paper (Wang and Veenstra, 1997), the rCx43 channel exhibits a cation-dependent anion permeability where the anion transiently binds to a cation as it encounters a cation at a fixed anionic site in the pore. However, the anion in the rCx43 pore is moving in the opposite direction to the cationic flux in a manner analogous to the model proposed by Borisova et al. (1986). As an example, extrapolating the γ_j-μ_{anion} plot (Fig. 5 *B*) to the y-intercept provides a maximum conductance estimate of 160.7 pS. Using the relative permeability coefficients for K^+, Cs^+, Na^+, TEA^+, and Cl^- and their respective ionic concentrations in the IPS, Cl^- would be expected to contribute about 19.7 pS to the total conductance. Assuming glutamate$^-$ is 5.28 times less permeable than Cl^-, which is the reciprocal of the $P_{glutamate}/P_{Cl}$ value in Table V, then glutamate$^-$ would be expected to contribute about 3.2 pS to the total conductance of the rCx40 channel. By assuming that the anion is forming anion-cation complexes in the pore, Cl^- and glutamate$^-$ should be reducing the channel conductance by this equivalent amount, which gives a predicted conductance of 141 and 157 pS respectively. These theoretical calculations are very close to the corresponding experimental γ_j values of 142 and 160 pS. This proposed mechanism is similar to one described by Franciolini and Nonner (1994) for an anion channel where cation permeation was dependent on the formation of transient cation-anion complexes over the entire length of the channel, and reducing the total charge flux below that sustainable by anions alone. Since net current is reduced by anion permeation, this interpretation is consistent with the reversal potentials obtained under asymmetric anion salt conditions and translates into P_Y/P_{Cl} coefficients which are the reciprocal of those listed in Table V. This is a testable hypothesis since anion permeability ratios will vary depending on salt concentration and on which permeant cation is present. Furthermore, there should be no anion conductance in the presence of an impermeant cation for the rCx40 pore and the maximum conductance should be achieved in the presence of an impermeant anion. However, such ions have yet to be identified for gap junction channels.

Specific ionic block of a connexin channel also has not been demonstrated previously. Experiments with TBACl strongly suggest that TBA^+ is capable of entering, but not traversing the rCx40 pore. Findings are presented (Fig. 3) which suggest that unilateral addition of only 2 or 5 mM TBACl leads to a block of rCx40 channel activity when the V_j polarity is net positive for the TBA^+-containing cell. This process is slowly reversible upon switching the V_j polarity to net negative with respect to the TBA^+-containing cell. This occurs without alteration of the single channel conductance for the events observed prior to or after removal of block. The concentration-dependence, kinetics (e.g., time to first opening after block), and V_j-dependence of TBA^+ block were not examined in detail in this investigation. The data presented demonstrate the reproducibility and reversibility of the observed phenomenon and are consistent with the proposed mechanism of action.

The results with TBA^+ and mannitol suggest that these two molecules are not permeable through the rCx40 pore. This is in contrast to the results with rCx43 where mannitol did not produce a sustained reversal potential in asymmetrical 115/30 mM LiCl. Brief records with symmetrical 115 mM TBACl also indicated the presence of rCx43 junctional channel activity although the nonjunctional membrane noise increased during the course of the experiments and eventually precluded the resolution of unitary junctional currents (Wang and Veenstra, 1997). TBA^+ has an effective ra-

dius of 4.94 Å and mannitol, being more linear and containing fewer carbon atoms, should be even smaller. Taken together, these results suggest that the higher conductance rCx40 channel has a smaller limiting pore radius than the rCx43 channel. Estimates of pore radius for rCx43 were 6.3 ± 0.4 Å (Wang and Veenstra, 1997), and the same approach (i.e., cation permeability ratios and the hydrodynamic equation) gives an estimate of 6.6 ± 0.7 Å for the rCx40 pore. These values are essentially indistinguishable from each other. Identification of the largest permeant and smallest impermeant cations for the rCx40 channel will ultimately provide the best estimate of pore size and allow direct comparison to other connexin channels. In the present investigations, the largest permeant monovalent cation used in the conductance and permeability measurements had a relative ion/pore radius of ≤0.65 according to the estimates of pore radius. As modeled in the rCx43 channel (Wang and Veenstra, 1997), the limiting radius of ≈6.6 Å for the rCx40 pore is sufficient to produce a greater reduction in the mobility of TMA^+ relative to the more hydrated Li^+, resulting in a switch of positions in the conductance ratio sequences ($Li^+ \simeq TMA^+$) for both channels.

In summary, our investigation of monovalent cation and anion permeability and conductance ratios leads to the conclusion that the rCx40 channel is not a simple aqueous pore. Monovalent cations apparently permeate through the pore in a partially hydrated state with reduced mobilities determined by the effective ionic radius relative to the limiting pore radius of ≈6.6 Å. The rCx40 channel appears to have a low anionic permeability which could be due to one or more fixed anionic sites within the pore. The mechanism of anion permeation remains to be definitively determined although all results suggest that formation of cation-anion complexes is probable. The differences in cation, anion, and molecular (mono-, tri-, and tetrasaccharide) permeabilities suggest that differences exist in charge composition and pore size for rCx40 and rCx43 channels. These results should provide a framework for future examination of structure-function differences among connexin channels in the pore-lining amino acid sequences.

The rat Cx40 transfected N2A cells were courteously provided by Dr. Eric C. Beyer, Washington University School of Medicine, St. Louis, MO 63110. We thank Mark G. Chilton for maintaining the N2A cell cultures. We wish to thank Dr. Peter R. Brink, Dept. of Physiology and Biophysics, SUNY Health Science Center, Stony Brook, NY 11794 for helpful discussions about the biophysical determinants of ionic permeability within a pore and Dr. Joseph D. Robinson for his helpful comments on the manuscript.

The research was supported by National Institute of Health grants HL-42220 and HL-45466.

Original version received 23 October 1995 and accepted version received 6 January 1997.

REFERENCES

Adams, D.J., T.M. Dwyer, and B. Hille. 1980. The permeability of endplate channels to monovalent and divalent metal cations. *J. Gen. Physiol.* 75:493–510.

Andersen, O.S. 1975. Ion-specificity of gramicidin channels. *In* International Biophysics Congress. Copenhagen, Denmark. 112. (Abstr.).

Anderson, J.L., and J.A. Quinn. 1974. Restricted transport in small pores. A model of steric exclusion and hindered particle motion. *Biophys. J.* 14:130–150.

Beblo, D.A., H.-Z. Wang, E.C. Beyer, E.M. Westphale, and R.D. Veenstra. 1995. Unique conductance, gating, and selective permeability properties of gap junction channels formed by connexin40. *Circ. Res.* 77:813–822.

Bennett, M.V.L., and D.C. Spray. 1965. Gap Junctions. Cold Spring Harbor Laboratory, Cold Spring Harbor, New York.

Beyer, E.C. 1993. Gap junctions. *Int. Rev. Cytol.* 137C:1–37.

Beyer, E.C., and R.D. Veenstra. 1994. Molecular biology and electrophysiology of cardiac gap junction proteins. *In* Handbook of Molecular and Cellular Physiology of Membrane Channels. C. Peracchia, editor. Academic Press, San Diego, CA. 379–401.

Blatz, A.L., and K.L. Magleby. 1984. Ion conductance and selectivity of single calcium-activated potassium channels in cultured rat muscle. *J. Gen. Physiol.* 84:1–23.

Borisova, M.P., R.A. Brutyan, and L.N. Ermishkin. 1986. Mechanism of anion-cation selectivity of amphotericin B channels. *J. Membr. Biol.* 90:13–20.

Bormann, J., O.P. Hamill, and B. Sakmann. 1987. Mechanism of anion permeation through channels gated by glycine and γ-aminobutyric acid in mouse cultured spinal neurones. *J. Physiol. (Lond.).* 385:243–286.

Brink, P.R., and S.F. Fan. 1989. Patch clamp recordings from membranes which contain gap junction channels. *Biophys. J.* 56:579–593.

Bruzzone, R., J.-A. Haefliger, R.L. Gimlich, and D.L. Paul. 1993. Connexin40, a component of gap junctions in vascular endothelium, is restricted in its ability to interact with other connexins. *Mol. Biol. Cell.* 4:7–20.

Caspar, D.L.C., D.A. Goodenough, L. Makowski, and W.C. Phillips. 1977. Gap junction structures. I. Correlated electron microscopy and x-ray diffraction. *J. Cell Biol.* 74:605–628.

Davis, L.M., H.L. Kanter, E.C. Beyer, and J.E. Saffitz. 1994. Distinct gap junction protein phenotypes in cardiac tissues with disparate conduction properties. *J. Am. Coll. Cardiol.* 24:1124–1132.

Dwyer, T.M., D.J. Adams, and B. Hille. 1980. The permeability of the endplate channel to organic cations in frog muscle. *J. Gen. Physiol.* 75:469–492.

Eisenman, G., J. Sandblom, and E. Neher. 1978. Interactions in cation permeation through the gramicidin channel Cs, Rb, K, Na, Li, Tl, H, and effects of anion binding. *Biophys. J.* 22:307–340.

Franciolini, F., and W. Nonner. 1987. Anion and cation permeabil-

ity of a chloride channel in rat hippocampal neurons. *J. Gen. Physiol.* 90:453–478.

Franciolini, F., and W. Nonner. 1994. A multi-ion permeation mechanism in neuronal background chloride channels. *J. Gen. Physiol.* 104:725–746.

Gourdie, R.G., N.J. Severs, C.R. Green, S. Rothery, P. Germroth, and R.P. Thompson. 1993. The spatial distribution and relative abundance of gap-junctional connexin40 and connexin43 correlate to functional properties of components of the cardiac atrioventricular conduction system. *J. Cell Sci.* 105:985–991.

Hertzberg, E.L., and R.G. Johnson. 1988. Gap Junctions. Alan R. Liss, Inc., New York.

Hess, P., J.B. Lansman, and R.W. Tsien. 1986. Calcium channel selectivity for divalent and monovalent cations. Voltage and concentration dependence of single channel current in ventricular heart cells. *J. Gen. Physiol.* 88:293–319.

Hille, B. 1975. Ionic selectivity of Na and K channels of nerve membranes. *In* Membranes: A Series of Advances, Vol. 3, Dynamic Properties of Lipid Bilayers and Biological Membranes. G. Eisenman, editor. Marcel Dekker, Inc., New York. 255–323.

Hille, B. 1992. Ionic Channels of Excitable Membranes. Sinauer Associates, Inc., Sunderland, MA.

Levitt, D.G. 1975. General continuum analysis of transport through pores. *Biophys. J.* 15: 533–551.

Levitt, D.G. 1991. General continuum theory for multiion channel II. Application to acetylcholine channel. *Biophys. J.* 59:278–288.

Loewenstein, W.R. 1981. Junctional intercellular communication. The cell-to-cell membrane channel. *Physiol. Rev.* 61:829–913.

Makowski, L., D.L.C. Caspar, W.C. Phillips, and D.A. Goodenough. 1977. Gap junction structures. II. Analysis of the x-ray diffraction data. *J. Cell Biol.* 74:629–645.

Manivannan, K., S.V. Ramanan, R.T. Mathias, and P.R. Brink. 1992. Multichannel recordings from membranes which contain gap junctions. *Biophys. J.* 61:216–227.

Myers, V.B., and D.A. Haydon. 1972. Ion transfer across lipid membranes in the presence of gramicidin A. II. The ion selectivity. *Biochem. Biophys. Acta.* 274:313–322.

Neher, E. 1975. Ionic specificity of the gramicidin channel and the thallous ion. *Biochem. Biophys. Acta.* 401:540–544.

Nightingale, E.R. 1959. Phenomenological theory of ion solvation. Effective radii of hydrated ions. *J. Phys. Chem.* 63:1381–1387.

Peracchia, C. 1973. Low resistance junctions in crayfish. II. Structural details and further evidence for intercellular channels by freeze-fracture and negative staining. *J. Cell Biol.* 57:66–80.

Ramanan, S.V., and P.R. Brink. 1993. Multichannel recordings from membranes which contain gap junctions. II. Substates and conductance shifts. *Biophys. J.* 65:1387–1395.

Renkin, E.M. 1954. Filtration, diffusion, and molecular sieving through porous cellulose membranes. *J. Gen. Physiol.* 38:225–243.

Robinson, R.A., and R.H. Stokes. 1955. Electrolyte Solutions. Academic Press, Inc., New York.

Sandblom, J., G. Eisenman, and E. Neher. 1977. Ionic selectivity, saturation and block in gramicidin A channels. I. Theory for the electrical properties of ion selective channels having two pairs of binding sites and multiple conductance states. *J. Membr. Biol.* 31: 383–417.

Spray, D.C., and J.M. Burt. 1990. Structure-activity relations of the cardiac gap junction channel. *Am. J. Physiol.* 258:C195–C205.

Veenstra, R.D., and P.R. Brink. 1992. Patch clamp analysis of gap junctional currents. *In* Cell-Cell Interactions: A Practical Approach. Stevenson, B., D.L. Paul, and W. Gallin, editors. IRL Press, Oxford, U.K. 167–201.

Wang, H.-Z., and R.D. Veenstra. 1997. Monovalent cation and anion selectivity sequences of the rat connexin43 gap junction channel. *J. Gen. Physiol.* 109:491–507.